

- 199, 1128 (1994); M. Mayrlleitner, R. Schafer, S. Fleischer, *Cell Calcium* **17**, 141 (1995).
8. A. A. Khan, J. P. Steiner, M. G. Klein, M. F. Schneider, S. H. Snyder, *Science* **257**, 815 (1992).
 9. O. Blondell, J. Takeda, H. Janssen, S. Seino, G. Bell, *J. Biol. Chem.* **268**, 11356 (1993).
 10. T. C. Sudhof, C. L. Newton, B. T. Archer III, Y. A. Ushkaryov, G. A. Mignery, *EMBO J.* **10**, 3199 (1991); C. A. Ross, S. K. Danoff, M. J. Schell, S. H. Snyder, A. Ullrich, *Proc. Natl. Acad. Sci. U.S.A.* **89**, 4265 (1992).
 11. N. L. Warner, A. W. Harris, G. A. Gutman, in *Membrane Receptors of Lymphocytes*, M. Seligmann, J. L. Preud'homme, F. M. Kourilsky, Eds. (North-Holland, Amsterdam, 1975), p. 203; A. DeFranco, M. Davis, W. E. Paul, in *B and T Cell Tumors: Biological and Clinical Aspects*, E. Vitetta, Ed. (Academic Press, New York, 1982), pp. 445–450; D. W. Scott, A. O'Garra, D. Warren, G. G. B. Klaus, *J. Immunol.* **139**, 3924 (1987); A. W. Boyd and J. W. Schrader, *ibid.* **126**, 2466 (1981); L. E. Benhamou, P.-A. Casenave, P. Sarthou, *Eur. J. Immunol.* **20**, 1405 (1990); J. Hasbold and G. G. B. Klaus, *ibid.*, p. 1685.
 12. C. Dive *et al.*, *Biochim. Biophys. Acta* **1133**, 275 (1992); Z. Darzynkiewicz *et al.*, *Cytometry* **13**, 795 (1992).
 13. Probes were inserts from plasmid subclones derived from a mouse placenta cDNA library (IP₃R1, AGTCT-TATTGTCAAAGCTTGCCCTTCCAAAGCCGCGAGATGAAGCA; IP₃R2, TTTCAACCAGCCACGATGGACAGTCAGTGTGTGAGACAAG; IP₃R3, CA-CTCCATCTGTCCCCACTACATGTGCCATAAA-TGTGGCAGCT). Total RNA was extracted from cells, and each lane contained ~25 µg of total RNA. An 18S RNA probe was used to normalize the quantity of the RNA.
 14. Antibodies to synthetic IP₃R peptides were prepared essentially as described [E. Harlow and D. Lane, *Antibodies, A Laboratory Manual* (Cold Spring Harbor Laboratory, Cold Spring Harbor, NY, 1988)]. Rabbit antibodies to the COOH-terminal amino acids of rat IP₃R1, IP₃R2, and IP₃R3—residues 2736 to 2749 (GHPPHM-NVNPQQPA), 2688 to 2701 (GSNTPHVNHHMPPH), and 2655 to 2670 (RRQLGFVDVQNCMSR), respectively—were prepared. An internal anti-IP₃R, residues 2432 to 2444 (VSEVSVPEILEED), was also used with similar results. Most of the ER IP₃R is cytoplasmic, with membrane-spanning loop regions in the lumen of the ER. A similar structure presumably exists in the IP₃R of the PM, with only a small region of the protein exposed extracellularly. As expected if the COOH-terminus of the putative PM IP₃R is cytoplasmic, no staining was observed in unpermeabilized cells. Accordingly, cells were permeabilized before staining with subtype-specific anti-IP₃R. Abbreviations for the amino acid residues are as follows: A, Ala; C, Cys; D, Asp; E, Glu; F, Phe; G, Gly; H, His; I, Ile; K, Lys; L, Leu; M, Met; N, Asn; P, Pro; Q, Gln; R, Arg; S, Ser; T, Thr; V, Val; W, Trp; and Y, Tyr.
 15. X. M. Sun, D. Dinsdale, R. T. Snowden, G. M. Cohen, D. N. Skilleter, *Biochem. Pharmacol.* **44**, 2131 (1992).
 16. D. J. McConkey *et al.*, *Arch. Biochem. Biophys.* **269**, 365 (1989); J. J. Cohen, *Semin. Immunol.* **4**, 363 (1992).
 17. A. W. Harris, *Exp. Cell Res.* **60**, 341 (1970); P. Ralph, R. Hyman, R. Epstein, I. Nakoinz, M. Cohn, *Biochem. Biophys. Res. Commun.* **55**, 1085 (1973); J. M. Harmon, M. R. Norman, B. J. Fowlkes, E. B. Thompson, *J. Cell. Physiol.* **98**, 267 (1979); W. V. Vedecis and H. D. Bradshaw Jr., *Mol. Cell. Endocrinol.* **30**, 215 (1983); M. Danielson, D. O. Peterson, M. R. Stallcup, *Mol. Cell. Biol.* **3**, 1310 (1983); L. M. Caron-Leslie and J. A. Cidlowski, *Mol. Endocrinol.* **5**, 1169 (1991).
 18. A. A. Khan and S. H. Snyder, unpublished data.
 19. I. Screpanti *et al.*, *J. Immunol.* **142**, 3378 (1989); C. D. Surh and J. Sprent, *Nature* **372**, 100 (1994).
 20. The polymerase chain reaction (PCR) was used to create DNA fragments corresponding to positions -81 to +9 of IP₃R1 and IP₃R3 mRNA. This region spans the translation initiation start site and shares no homology between the two receptors. An upstream primer (IP₃R1, AAGGAAGCTAGCGGCGCGACTA-CAAAGGATTGCA; IP₃R3, AAGGAAGCTAGCGGCGCGAGCGCGCTCAGTCTCT) and a downstream primer (IP₃R1, AAGGAAGCTAGCGGCGCG-GACTACAAGGATTGCA; IP₃R3, AAGGAAGCT-AGCGGCGCTCAGGCGAGGCTTGGC) were used in a PCR. As templates for the IP₃R3 and IP₃R1 antisense and sense constructs, cDNA for the IP₃R3 and rat brain cDNA for the IP₃R1 were used, respectively. For creation of the constitutive constructs, the amplified DNA fragments were digested with Not I and subcloned into pOPRSVI (Stratagene) that had been linearized with the same enzyme. pOPRSVI is part of the LacSwitch Inducible Mammalian Expression System. The constitutive expression of pOPRSVI was turned off by cotransfection of the eukaryotic Lac repressor-expressing vector p3'SS. Several clones were analyzed by DNA sequencing to identify constructs with inserts in the antisense and sense orientations. The dexamethasone-inducible constructs were prepared in the same fashion except that the amplified DNA fragments and vector pMAMneo (Clontech) were digested with Nhe I. Dexamethasone treatment activated expression of IP₃R3 antisense in the dexamethasone-inducible pMAM plasmid constructs and inhibited dexamethasone-induced increases in IP₃R3 protein (Fig. 4A). In the dexamethasone-inducible IP₃R3 antisense-transfected cells, immunoblot analysis with antiserum to IP₃R3 revealed a reduction in amounts of IP₃R3 protein relative to noninduced control cells, whereas amounts of IP₃R1 in control and dexamethasone-treated IP₃R3 antisense cells were similar (Fig. 4A). S49 cells constitutively expressing IP₃R3 antisense had low resting amounts of IP₃R3 that did not increase with dexamethasone exposure.
 21. Relative amounts of DNA synthesis were measured in transfected cell lines after dexamethasone treatment by culturing 10⁵ cells in 0.5 ml of medium with 1 µCi of [³H]thymidine. After 18 hours, cells were lysed onto glass filters for scintillation counting. DNA synthesis data represent the mean counts per minute ± SD for triplicate determinations and are representative of four experiments. DNA synthesis was measured after 4 days of incubation in 10 nM dexamethasone for cell lines transfected with the dexamethasone-inducible plasmid pMAM and after 2 days of incubation in 0.1 µM dexamethasone for cell lines transfected with the constitutively expressing plasmid pOPRSVI.
 22. Transfected S49 cells in culture medium (RPMI 1640 containing 10% heat-inactivated FBS), either untreated or treated with 0.1 µM dexamethasone for 2, 3, or 4 days, were loaded with 2 µM Indo-1 AM (Molecular Probes) by incubation for 45 min at 37°C in 145 mM NaCl, 5 mM KCl, 0.1 mM MgCl₂, 1 mM CaCl₂, 5.5 mM glucose, and 15 mM Hepes (pH 7.5). Indo-1 fluorescence was analyzed with a FACStarplus flow cytometer (Becton Dickinson). The fluorescence data were converted to [Ca²⁺]_i values [P. S. Rabinovitch, C. H. June, A. Grossmann, J. A. Ledbetter, *J. Immunol.* **137**, 952 (1986)]. Electric grays were drawn to separate live and dead cells. The use of blue and red to indicate cells containing low and high calcium concentrations was based on lines of demarcation between live and dead populations of cells that most clearly resolved the low-calcium (78 nM) and high-calcium (409 nM) groups of cells, and it highlights the association between changes in light scatter and increases in [Ca²⁺]_i after dexamethasone treatment. Loss of membrane integrity occurs late in apoptosis. [Ca²⁺]_i measurement in cells with changes in light scatter reflects only those cells whose membrane integrity was still intact and excluded trypan blue.
 23. J. W. Putney Jr., *Cell Calcium* **7**, 1 (1986); R. S. Lewis and M. D. Cahalan, *Cell Regul.* **1**, 99 (1989).
 24. L. Meynard *et al.*, *Science* **257**, 217 (1992); M. L. Gougeon and L. Montagnier, *ibid.* **260**, 1269 (1993); C. J. Li, D. J. Friedman, C. Wang, V. Metelev, A. B. Pardee, *ibid.* **268**, 429 (1995).
 25. We thank G. Bell for IP₃R3 cDNA and C. Williams for pathology photography. Supported by the W. C. Keck Foundation and by USPHS grants AI-20922 and AI-37934 (to M.J.S.), MH43040 (to C.A.R.), and MH-18501 and Research Scientist Award DA-00074 (to S.H.S.).

21 December 1995; accepted 29 April 1996

The POU Factor Oct-6 and Schwann Cell Differentiation

Martine Jaegle, Wim Mandemakers, Ludo Broos, Ronald Zwart, Alar Karis, Pim Visser, Frank Grosveld, Dies Meijer*

The POU transcription factor Oct-6, also known as SCIP or Tst-1, has been implicated as a major transcriptional regulator in Schwann cell differentiation. Microscopic and immunohistochemical analysis of sciatic nerves of Oct-6^{-/-} mice at different stages of postnatal development reveals a delay in Schwann cell differentiation, with a transient arrest at the promyelination stage. Thus, Oct-6 appears to be required for the transition of promyelinating cells to myelinating cells. Once these cells progress past this point, Oct-6 is no longer required, and myelination occurs normally.

Schwann cells are involved in the trophic support and insulation of axons and are the only glial cell type in peripheral nerve trunks. The two types of Schwann cells, myelinating Schwann cells associated with axons greater than 1 µm in diameter and nonmyelinating cells associated with multiple lower caliber axons, both differentiate from neural crest-derived Schwann cell precursors. Myelination initiation correlates

with axon diameter and is governed by axonal signals that are as yet not understood (1).

A number of transcription factors have been proposed to be involved in Schwann cell differentiation and myelination (2). Prominent among those is the POU domain transcription factor Oct-6 (also known as SCIP or Tst-1) (3). The Oct-6 protein is expressed in the Schwann cells of the sciatic nerve and the sympathetic trunk from embryonic day 16 (E16) onward (4). During postnatal nerve development, the expression of Oct-6 mRNA is gradually down-regulated and extinguished, with only spo-

Medical Genetics Center, Department of Cell Biology and Genetics, Erasmus University, Post Office Box 1738, 3000 DR Rotterdam, Netherlands.

*To whom correspondence should be addressed. E-mail: meijer@gen.tgg.eur.nl

radic expression in Schwann cells of the adult nerve (5). In vitro and transgenic mouse experiments have suggested that Oct-6 acts as a negative transcriptional regulator and as a general repressor of myelin genes in proliferating Schwann cells (6). By inference, Oct-6 was postulated to be involved in embryonic Schwann cell proliferation and to regulate the correct number of Schwann cells in the peripheral nerves. In the absence of Oct-6 gene function, one

prediction of this model is that Schwann cells will differentiate prematurely and their numbers will be reduced.

To elucidate the role of the Oct-6 gene in Schwann cell differentiation, we interrupted the DNA binding domain of the mouse Oct-6 locus through homologous recombination in embryonic stem (ES) cells, with a β -galactosidase-neomycin fusion gene (7) (Fig. 1). Two different Oct-6^{+/-} ES cell lines produced chimeric animals and had

high frequencies of germline transmission. Identical results were obtained from both lines. Heterozygote animals were healthy and had no readily apparent abnormalities. Analysis of β -galactosidase activity in these animals confirmed the previously described Oct-6 expression pattern (3, 4, 8).

Mice homozygous for the mutated Oct-6 allele were produced at normal Mendelian ratios and developed to term and showed no gross anatomical abnormalities. Most Oct-6^{-/-} pups died soon after birth, but 2 to 4% survived for a longer period. From postnatal day 5 (P5) onward, mutant animals could be identified by their smaller size and occasional tremors in the second postnatal week.

To determine whether Schwann cells were affected in the Oct-6^{-/-} mice, immunohistochemical analysis was performed (8). Normally, myelinating Schwann cells coordinately express myelin genes such as those encoding protein zero (P₀), peripheral myelin protein (PMP-22), myelin basic protein (MBP), and myelin-associated glycoprotein

Fig. 1. Targeted disruption of the Oct-6 gene. **(A)** Targeting strategy. Schematic representation of the mouse Oct-6 gene (middle). The thick black line represents the transcribed part of the Oct-6 locus, which is encoded by a single exon. The open box represents the open reading frame, and the hatched box represents the POU domain. A DNA fragment containing a β -galactosidase-neomycin fusion gene preceded by an internal ribosome entry site (IRES) (7) (gray and striped boxes) was inserted into the Xho I site of the Oct-6 gene, thereby disrupting the DNA binding domain of the Oct-6 protein (top). A schematic representation is also shown of the mutant allele, indicating the position of the probes that were used to identify homologous recombinant ES cell lines (bottom). **(B)** Southern blot of Eco RI-restricted DNA, showing a 4.6-kb mutant allele band and a 6.8-kb wild-type allele band detected by probe 2. The mutant allele expresses a 6.9-kb bicistronic mRNA under control of the endogenous Oct-6 promoter and its regulatory sequences. No full-length Oct-6 protein can be produced from this mRNA.

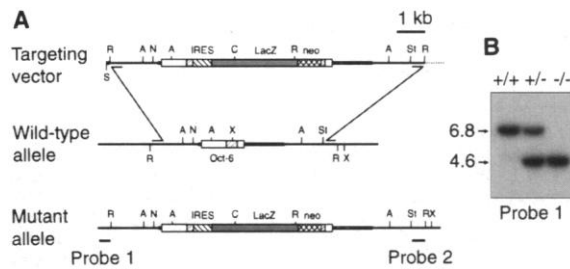


Fig. 2. Immunohistochemical analysis of wild-type versus Oct-6^{-/-} mutant sciatic nerves. Sciatic nerves of 18 days postcoitum embryos **(A and B)** and P8 **(C and D)** and P14 pups **(E and F)** were analyzed for the expression of the Oct-6 protein (green fluorescent signal) and the myelin protein P₀ (red fluorescent signal) (9). Wild-type and Oct-6^{-/-} nerves express basal levels of the P₀ protein at E18 **(A and B)**. A few cells express already high levels of P₀ **(A, white arrows)**. At P8 and at P14, high levels of P₀ expression are seen in wild-type nerve **(C and E)**, whereas in mutant nerve, only a small number of Schwann cells express high levels of the P₀ protein **(D and F, white arrows)**. Immunohistochemical analysis of paraffin sections was as described (8). The bar represents 50 μ m.

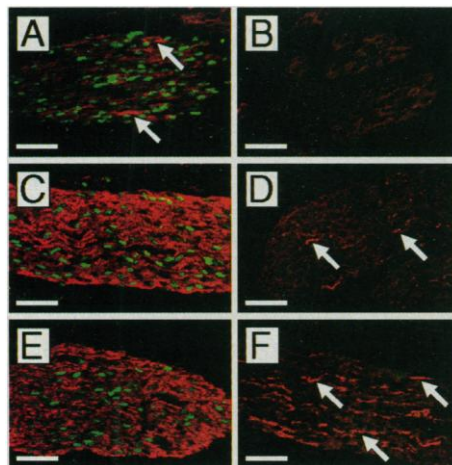


Fig. 3. Expression of early and late myelin markers in the sciatic nerves of Oct-6^{-/-} and Oct-6^{+/-} animals. **(A)** Protein immunoblot analysis of protein extracts from mutant and heterozygote sciatic nerves at P1, P8, P11, and P14. The blots were probed with antibodies to P₀, CNP, MBP, and NF-M. The amount of protein is normalized for the NF-M signal. The relative molecular mass is indicated by M_r . **(B)** Semiquantitative PCR analysis of expression levels of MAG, PMP-22, and MBP in P14 Oct-6^{+/-} and Oct-6^{-/-} sciatic nerves. For each gene, amplification of hypoxanthine phosphoribosyl-transferase (HPRT) cDNA was used as an internal control in every second panel. Samples were taken at cycles 20 (lane 1 and 5), 22 (lane 2 and 6), 24 (lane 3 and 7), and 26 (lane 4 and 8).

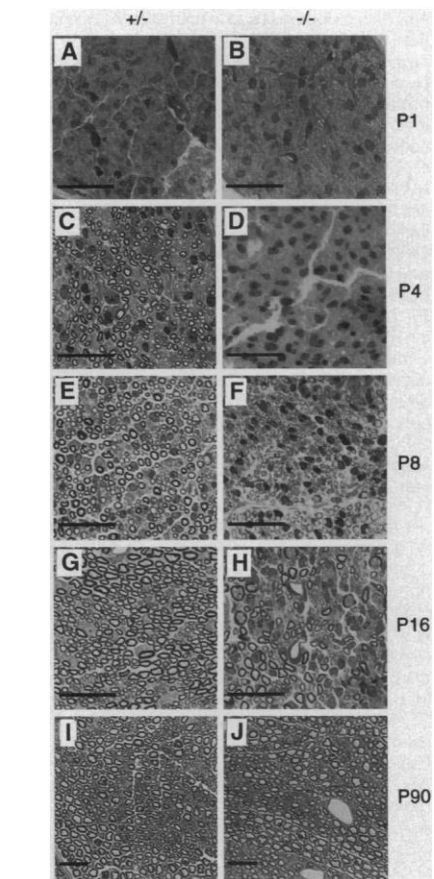
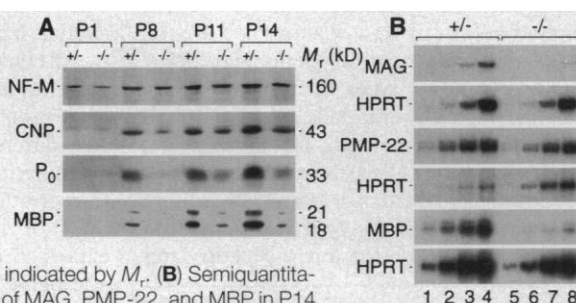


Fig. 4. Microscopic cross sections of sciatic nerves of Oct-6^{+/-} and Oct-6^{-/-} animals at different stages of postnatal development. The left panels were derived from Oct-6^{+/-} animals, and the right panels were derived from Oct-6^{-/-} animals. Semithin sections (1 μ m) of Epon-embedded material were stained with methylene blue. The age of the animal is indicated on the right. The bar in each panel represents 25 μ m.

(MAG). Examination of E18 nerves showed that P_0 expression levels were normal, and no abnormalities in either the number of Schwann cells or the shape of their nuclei were apparent (Fig. 2, A and B, and Fig. 4, A and B). However, P8 and P14 sciatic nerves of $-/-$ animals appeared to be defective in myelination. The nerves revealed reduced levels of P_0 expression relative to the highly P_0 -positive nerves of $+/+$ littermates (Fig. 2). Some $Oct-6^{-/-}$ Schwann cells express normal, high levels of P_0 (Fig. 2D), but most express little P_0 . At P14, the number of Schwann cells that express high levels of P_0 had increased (Fig. 2F).

Protein immunoblotting and semiquantitative reverse transcriptase-polymerase chain reaction (RT-PCR) were used to examine the expression levels of a number of early and late myelin markers in the sciatic nerve at different stages of postnatal development (9). Less than normal P_0 and MBP levels were found in the mutant nerve (Fig. 3A). Early expression of 2',3'-cyclic nucleotide 3'-phosphodiesterase (CNP) protein at P1 was not affected (Fig. 3A), but the postnatal increase was less. We also examined the mRNA levels of the genes encoding myelination markers PMP-22, MAG, and MBP (Fig. 3B) and found them to be

reduced. These expression data suggest that in $Oct-6^{-/-}$ animals, nerve myelination is delayed but not completely blocked. Alternatively, it is possible that a number of Schwann cells differentiate normally, whereas the rest are blocked at an early stage of differentiation.

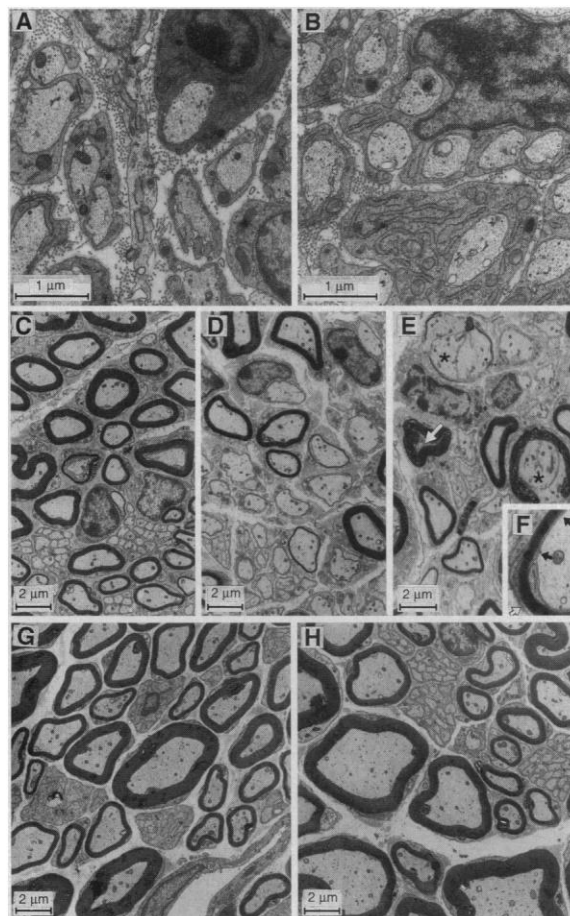
To distinguish between these possibilities, we examined the microscopic structure of sciatic nerves at different stages of postnatal development (10). Normally, only a few myelinating Schwann cells were observed at birth, with extensive myelination visible at P4 and P8 (Fig. 4, A, C, and E). At P16, myelination was well advanced, with many fully myelinated axons (Fig. 4, G and I). However, in the $Oct-6^{-/-}$ nerve, no evidence of myelination was seen until the second week of postnatal development (Fig. 4, B, D, F, and H). In adult $Oct-6^{-/-}$ nerves, myelination appeared complete (Fig. 4J).

Electron microscopic analysis of 80-nm sections of sciatic nerves from $-/-$ and $+/-$ mice revealed no differences at P1. Schwann cells were actively ensheathing axons, and promyelin figures were observed in which Schwann cells had acquired a 1:1 relation with an axon. There was a normal deposition of collagen fibrilles, and $Oct-6^{-/-}$ and $Oct-6^{+/-}$ Schwann cells produced

a basement membrane (Fig. 5, A, B, and F). In wild-type P16 nerves, most large-caliber axons were myelinated, whereas $Oct-6^{-/-}$ P16 nerves showed an immature phenotype with promyelin figures with only the larger axons myelinated. Schwann cells that had myelinated a single, large caliber axon appeared normal, with an uncompacted periaxonal membrane and tightly packed myelin membranes (Fig. 5F). Very sporadically, abnormal myelin figures were observed that showed several large axons associated with a myelinating Schwann cell (Fig. 5E). These Schwann cells showed severely disrupted myelination, as evidenced by their failure to wrap myelin around the axon, resulting in disorganized myelin sheaths. Such Schwann cells started myelination before a 1:1 relation with an axon was established. Sometimes myelination was observed in the absence of an axon (Fig. 5E). In adult $Oct-6^{-/-}$ animals, nerve myelination was complete (Fig. 5, G and H).

These data demonstrate that in $Oct-6^{-/-}$ mice there is a delay in the onset of myelination and not a block in the differentiation of Schwann cells. This delay is characterized by a transient arrest of Schwann cells at the promyelin stage. Once cells progress past this stage, myelination occurs normally, which indicates that $Oct-6$ is not involved in the execution of the terminal differentiation program. These results are in contrast with transgenic studies in which a dominant negative form of $Oct-6$ under transcriptional control of the P_0 promoter results in an early onset of myelination and hypermyelination. This discrepancy may suggest separate functions for $Oct-6$ protein in early and late Schwann cell development, as discussed by Weinstein *et al.* (6, 11). Our results suggest that $Oct-6$ exerts its function in Schwann cell development through the regulation of genes that are involved in embryonic Schwann cell axon interactions that govern the transition from a promyelin cell to a myelinating Schwann cell. Exactly which genes are regulated by $Oct-6$ and how this process mediates the progression of Schwann cell differentiation require further study.

Fig. 5. Ultrastructure of sciatic nerves at different stages of postnatal development. Shown is the ultrastructural appearance of an $Oct-6^{+/-}$ (A) and $Oct-6^{-/-}$ (B) nerve at P1. Ensheathing and promyelin cells are visible in both nerves. The darker cell in the upper right part of (A) has made the first wrap around its axon. (C) $Oct-6^{+/-}$ nerve at P16. (D and E) Representative sections of an $Oct-6^{-/-}$ nerve at P16. Panel (D) illustrates the normal but immature appearance of an $Oct-6^{-/-}$ nerve at P16, and (E) illustrates the sporadic abnormalities observed in mutant nerves. The open arrow indicates myelination in the absence of an axon. The asterisks indicate large axons associated with a myelinating Schwann cell. (F) Mutant Schwann cell that has produced a normal myelin sheath. The solid arrows indicate an uncompacted periaxonal membrane. The white arrow points at an apparently normal basement membrane. Also shown are representative sections of adult heterozygous (G) and mutant (H) nerves.



REFERENCES AND NOTES

1. K. R. Jessen *et al.*, *Neuron* **12**, 509 (1994); K. R. Jessen and R. Mirsky, *Curr. Opin. Neurobiol.* **2**, 575 (1992); N. M. LeDourain, C. Ziller, G. F. Couly, *Dev. Biol.* **159**, 24 (1993); H. J. Weinberg and P. S. Spencer, *J. Neurocytol.* **4**, 395 (1975).
2. G. Lemke, in *Molecular Neurobiology*, Z. W. Hall, Ed. (Sinauer, Sunderland, MA, 1992), p. 281; C. Kiousi, M. K. Gross, P. Gruss, *Neuron* **15**, 553 (1995); P. Topilko *et al.*, *Nature* **371**, 796 (1994); E. S. Monuki, R. Kuhn, G. Weinmaster, B. D. Trapp, G. Lemke, *Science* **249**, 1300 (1990).
3. E. S. Monuki, G. Weinmaster, R. Kuhn, G. Lemke, *Neuron* **3**, 783 (1989); X. He *et al.*, *Nature* **340**, 35 (1989); N. Suzuki *et al.*, *EMBO J.* **9**, 3723 (1990); D.

- Meijer *et al.*, *Nucleic Acids Res.* **18**, 7357 (1990).
- R. Zwart, thesis, Erasmus University, Rotterdam (1996).
 - S. S. Scherer *et al.*, *J. Neurosci.* **14**, 1930 (1994).
 - E. S. Monuki, R. Kuhn, G. Lemke, *Mech. Dev.* **42**, 15 (1993); D. E. Weinstein, P. G. Burrola, G. Lemke, *Mol. Cell. Neurosci.* **6**, 212 (1995); X. He *et al.*, *Mol. Cell. Biol.* **11**, 1739 (1991).
 - P. Mountford *et al.*, *Proc. Natl. Acad. Sci. U.S.A.* **91**, 4303 (1994). Oct-6 genomic clones were isolated from a 129-genomic phage library and mapped with the use of several restriction enzymes. The targeting vector was linearized at the single Sal I site and electroporated into E14 ES cells maintained in BRL cell conditioned medium in the presence of Leukemia Inhibitory Factor. After selection in G418, correct replacement events were identified by Southern blot hybridization with the use of an internal 3' probe and an external 5' probe. Homologous recombination events had occurred in 15 of 51 G418-resistant ES cell lines. A number of these lines were karyotyped, and two cell lines with the correct number of chromosomes were injected in C57BL/6 blastocyst embryos. Both lines resulted in germline transmission. Heterozygous offspring were crossed to C57BL/6 mice and backcrossed at the F₂ generation.
 - R. Zwart, L. Broos, G. Grosveld, D. Meijer, *Mech. Dev.* **54**, 185 (1996).
 - Sciatic nerves were isolated from mutant mice and heterozygote littermates. One nerve was used for

protein immunoblotting and another was used to isolate RNA. Nerves for protein immunoblotting were homogenized in sample buffer and loaded on a 15% (for P₀ and MBP) or 8% [for CNP and neurofilament medium chain (NF-M)] SDS-polyacrylamide gel. The gels were electroblotted on filters and further processed according to standard procedures. P₀ monoclonal antibody P07 was provided by J. J. Archelos [J. J. Archelos *et al.*, *J. Neurosci. Res.* **35**, 46 (1993)]. Other monoclonal antibodies were obtained from Boehringer Mannheim (MBP), Sigma (CNP), and Amersham (NF160). For RT-PCR, RNA was extracted with the LiCl-urea method and reverse-transcribed into cDNA with oligo(dT) and hexamer primers. Excess primers were removed on a Centricon C-30 (Amicon) concentrator. For MBP amplification, we used cDNA generated from P8 sciatic nerve RNA. After 20-fold dilution, polymerase chain reaction (PCR) amplification was performed by use of the Expand long template PCR system (Boehringer Mannheim). Each amplification cycle comprised 30 s at 94°C, 1 min at 55°C, and 1 min at 68°C. After the 10th amplification cycle, the extension time was increased with 20-s increments. Samples were taken at cycles 20, 22, 24, and 26. The following primers were used: MAG: 5'-primer GCCACGGTCATCTATGAGAGTCAGC and 3'-primer GGTGCCAGAGAT-TCTGAATTCGG; HPRT: 5'-primer CACGAGACTA-GAACACCTGC and 3'-primer GCTGGTGAAAAG-GACCTCT; PMP-22: 5'-primer AACTGCTACTC-CTCATCAGTGAG and 3'-primer CAGGATCACAT-

AGATGATACCACTG; and MBP: 5'-primer ACTCA-CACACGAGAAGTACCCA and 3'-primer CCAGCT-AAATCTGCTGAGGG. The amplified fragments yielded bands of 605 bp for MAG, 316 bp for PMP-22, 249 bp for HPRT, and 170 bp for MBP. Amplification products were separated on a 4% denaturing polyacrylamide gel, and signals were measured with a Molecular Dynamics phosphorimager.

- Animals were perfused with phosphate-buffered saline, pH 7.2, for 3 min followed by fixative (3% paraformaldehyde and 1% glutaraldehyde buffered by 100 mM cacodylate at pH 7.2) for 10 min. Nerves were dissected, cut into smaller pieces, and fixed overnight in the same fixative. After postfixation in 1% osmium tetroxide, the sample was embedded in Epon. Ultra-thin sections were stained with uranyl acetate and lead citrate. Sections were examined and photographed with a Philips CM100 electron microscope.
- R. Mirsky and K. R. Jessen, *Curr. Opin. Neurobiol.* **6**, 89 (1996).
- We are grateful to D. Bootsma for his support, to E. Dzierzak for critical comments on the manuscript, and to M. Kuit, T. de Vries Lentsch, R. Koppenol, and R. Willemse for photography. We gratefully acknowledge J. Archelos for P₀ antibodies and L. Braam for animal care. All animal experiments were carried out under license 132-95-03 (Institutional Animal Care and Use Committee, Erasmus University).

1 March 1996; accepted 5 June 1996

Spinal Cord Repair in Adult Paraplegic Rats: Partial Restoration of Hind Limb Function

Henrich Cheng,* Yihai Cao, Lars Olson

Complete spinal cord gaps in adult rats were bridged with multiple intercostal nerve grafts that redirected specific pathways from white to gray matter. The grafted area was stabilized with fibrin glue containing acidic fibroblast growth factor and by compressive wiring of posterior spinal processes. Hind limb function improved progressively during the first 6 months, as assessed by two scoring systems. The corticospinal tract regenerated through the grafted area to the lumbar enlargement, as did several bulbospinal pathways. These data suggest a possible repair strategy for spinal cord injury.

Treatment that promotes functional regeneration across a complete spinal cord transection in humans does not exist. In animal experiments (1), recovery after incomplete spinal cord lesions has been achieved in mature animals treated with myelin-associated protein antibodies, whereas recovery after complete lesions has been shown in neonates (2). To avoid ambiguity and to model the most severe clinical scenario, we studied adult rats with complete surgical transection of the spinal cord, including removal of 5 mm of the cord

at vertebra T8. Histology of excised pieces of spinal cord demonstrated complete transection (Fig. 1A). We then proceeded with a repair strategy (3).

We used peripheral nerve implants (4) to bridge the gap in the spinal cord (Fig. 1, B and C, and Fig. 2B) and found that the use of multiple fine nerve implants (18 nerves to bridge one gap) gave better precision than the use of fewer thicker nerves. To evade oligodendroglial proteins that inhibit axon regeneration (5), we rerouted regenerating pathways from nonpermissive white to permissive gray matter (6). The peripheral nerve bridges thus redirected descending motor pathways from proximal white to distal gray matter and ascending pathways from distal white to proximal gray matter (Fig. 1E), according to the specific anatomy of rat descending and ascending pathways (7). To stabilize the lesioned area and the peripheral nerve bridges, we filled the grafted area with a fibrin-based tissue

glue that does not impair nerve fiber growth (8) and fixed the vertebral column in dorsiflexion by wiring (9).

Acidic fibroblast growth factor (aFGF) is a normal spinal cord constituent (10). Because it lacks a signal sequence, aFGF is thought to be sequestered within cells and released only after damage. Consequently, FGF may be involved in repair (11). It also decreases gliosis and enhances nerve fiber development in spinal cord grafts (12). Mixing aFGF into fibrin glue allows slow release of the factor (13).

Animals were followed over time for signs of functional recovery and rated by two independent, blinded observers using the combined behavioral score (CBS) (14) and the open-field walking score (OFWS) (15). Key responses were videotaped. Hind limb function in animals subjected to the repair procedure improved significantly, beginning 3 weeks after operation and continuing through the 1 year of observation (Fig. 1D). Animals subjected to unilateral treatment also improved, although to a lesser degree. Animals in four different control groups [transection only ($n = 14$), cord removal only ($n = 5$), white matter-to-white matter bridging ($n = 3$), and omission of aFGF ($n = 2$)] did not improve (Fig. 1D). Improvement was manifest as appearance of a functional posture in hind limbs (usually flexion at hips and then knees and then dorsiflexion at ankles). In controls, hind limbs remained extended and externally rotated. Improvement was symmetrical in six cases (28%) and asymmetrical in the rest. Locomotion involved four-limbed stepping (Fig. 2, H through J). Hind limbs

H. Cheng, Department of Neuroscience, Karolinska Institute, S-171 77 Stockholm, Sweden, and Department of Neurosurgery, Neurologic Institute, Veterans General Hospital-Taipei and Division of Surgery, National Yang-Ming University, Taiwan.

Y. Cao, Department of Cell and Molecular Biology, Karolinska Institute, S-171 77 Stockholm, Sweden.

L. Olson, Department of Neuroscience, Karolinska Institute, S-171 77 Stockholm, Sweden.

*To whom correspondence should be addressed. E-mail: henrich.cheng@neuro.ki.se.